

Searching for quark cores with binary neutron star inspirals

Hsin-Yu Chen,^{1,*} Paul M. Chesler,^{1,†} and Abraham Loeb^{1,‡}

¹*Black Hole Initiative, Harvard University, Cambridge, Massachusetts 02138, USA*

We study the feasibility of detecting quark matter cores in merging neutron stars with ground-based gravitational-wave detectors. We focus on models with a sharp hadronic/quark matter interface, and assume a uniform distribution of neutron stars in the mass range $[1, 2]M_\odot$. We find that the existence of quark matter cores can be confirmed at the 70% confidence level with as few as several tens of detections. Likewise, with such a sample, we find that some models of quark matter cores can be excluded with high confidence.

Introduction.—The discovery of binary neutron star mergers (BNSs) by Advanced LIGO-Virgo [1] has ushered an era of multimessenger astronomy [2]. BNSs also provide a unique laboratory to study the equation of state (EoS) of Quantum Chromodynamics (QCD) matter, which at densities beyond the nuclear saturation density is largely unknown. Already, the single event GW170817 indicates a relatively soft EoS [3, 4]. Advanced LIGO-Virgo is expected to observe tens to hundreds of BNSs in the next few years [5], substantially improving constraints on the EoS of dense QCD matter over time (see *e.g.* [6–10]).

At asymptotically high densities, where perturbation theory is reliable, QCD predicts the existence of a deconfined phase of quark matter (QM), whose properties are very different from matter at nuclear densities (see *e.g.* [11]). It is natural to speculate that there exists a phase transition separating these two states of matter. A phase transition can result in hybrid neutron stars (HNS), where there is a QM core surrounded by a mantle of hadronic matter (see *e.g.* [12–20]). QM can also be produced during post-merger dynamics [21, 22]. A tantalizing question arises as to whether the effects of QM be observed with gravitational wave (GW) detectors. If so, what are the observable signatures of the phase transition? How many mergers must one observe before the presence of a phase transition can be confidently established? These are the questions we seek to address.

We focus on QM scenarios most easily observable with current GW detectors. As no obvious sign of post-merger dynamics were recorded in GW170817, likely due to post-merger dynamics being outside of LIGO’s frequency bandwidth, we choose to study the effects of HNSs during the inspiral phase of NS mergers. Additionally, we focus on HNSs with a sharp transition between hadronic and QM, meaning those without a mixed phase. This scenario arises when the surface tension of the hadronic/QM interface is large [16].

The presence of a QM core can have dramatic effects on mass-radius (MR) curves, with the nature of the modification depending on the discontinuity in the energy density (*i.e.* latent heat) and the speed of sound [17, 18, 23, 24]. For illustrative purposes, Fig. 1 shows the MR curve for the MPA1 hadronic EoS of Ref. [25] to-

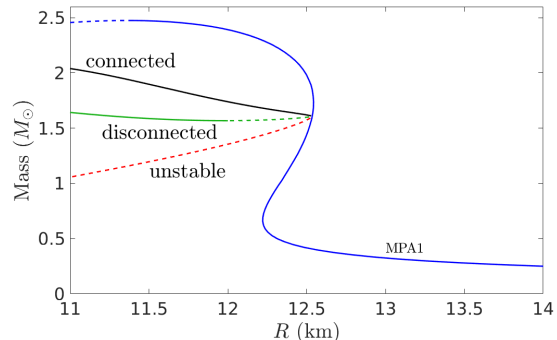


FIG. 1. An example of MR curves with and without a phase transition. The critical mass for the hybrid branch is $m_c = 1.6M_\odot$, beyond which QM cores exists. Regions with positive slope are unstable and shown as dashed lines.

gether with hybrid MR curves generated via a constant sound speed QM EoS. If the latent heat is large, HNSs are unstable to collapse and the stable branch of the MR curve terminates at some mass m_c , which is the mass where QM is first nucleated [13, 14]. For smaller latent heats, the resulting HNSs can have both connected and disconnected MR curves. Crucial to our analysis is the fact that the slope of hybrid branch of the MR curve need not be the same as that of the hadronic branch.

We focus on mergers with component masses in the $[1, 2]M_\odot$ range. There are two reasons for doing this. First, the heaviest observed neutron stars (NSs) have masses $2.01 \pm 0.04M_\odot$ [26] and $2.17 \pm 0.1M_\odot$ [27]. Because $2M_\odot$ NSs are evidently stable, astrophysical processes such as supernova and NS mergers presumably cannot produce black holes lighter than $2M_\odot$. Likewise, $\mathcal{O}(M_\odot)$ primordial black holes are not expected to be abundant (see for example [28]). It is therefore reasonable to surmise that all mergers with components in the $[1, 2]M_\odot$ range are BNSs. If the BNS detections are contaminated by neutron star-black hole mergers, significant biases in measured radii can be introduced [29]. Second, in the $[1, 2]M_\odot$ range the vast majority of viable hadronic EoS yield roughly constant MR curves (see for example Fig. 10 of Ref. [30]). This should be contrasted with the kink at critical mass m_c shown in Fig. 1. Restricting our

Model	$p_0(\text{km})$	$p_1(M_\odot)$	$p_2(\text{km}/M_\odot)$	$p_3(\text{km}/M_\odot)$
A	12.5	2.0	0.3	0.0
B	12.5	1.5	0.3	-0.7
C	12.5	1.8	0.8	-0.3
D	12.5	1.8	0.6	-5.0

TABLE I. Parameters chosen for the four piecewise hadronic NS MR curves.

attention to the $[1, 2]M_\odot$ range therefore allows us to use abrupt changes in MR curves – kinks – as an identifier for the phase transition, with the location of the kink corresponding to the critical mass m_c . As we shall see below, kinks in MR curves readily manifests themselves in GW observables, and can be seen with a large enough collection of events.

Simulations.— We construct an ensemble of simulated BNSs. Input data consists of the NS masses m_1 and m_2 and the NS MR curve. As the mass distribution of NSs outside the Milky Way is unknown, we choose m_1 and m_2 uniformly distributed in $[1, 2]M_\odot$, with $m_1 \geq m_2$. Additional GW observables we employ are the chirp mass $\mathcal{M} \equiv (m_1 m_2)^{3/5} / (m_1 + m_2)^{1/5}$, and the mass weighted tidal deformability

$$\tilde{\Lambda} \equiv \frac{16}{13} \frac{(m_1 + 12m_2)m_1^4 \Lambda_1 + (m_2 + 12m_1)m_2^4 \Lambda_2}{(m_1 + m_2)^5}, \quad (1)$$

where Λ_1 and Λ_2 are the tidal deformabilities of the individual NSs. $\tilde{\Lambda}$ is determined from the MR curve and the masses m_1 and m_2 . This follows from the universal relationship between each NS’s compactness $C \equiv m/R$, and tidal deformability Λ , which reads [15, 31]

$$C = a_0 + a_1 \log \Lambda + a_2 \log^2 \Lambda, \quad (2)$$

where $a_0 = 0.3617$, $a_1 = -0.03548$ and $a_2 = 6.194 \times 10^{-4}$. Eq. (2) holds at the 7% level or better for both purely hadronic NSs and HNSs [32]. Eq. (2) can be inverted to find $\Lambda(C)$, which upon substituting into Eq. 1 yields $\tilde{\Lambda}$ in terms of m_1 and m_2 and the NS radii R_1 and R_2 .

Our analysis below is unable to resolve detailed structure in MR curves. Because of this, to generate simulated events we use the piecewise linear MR curves

$$\mathcal{R}(m|p_0, p_1, p_2, p_3) \equiv \begin{cases} p_2(m - p_1) + p_0, & m < p_1, \\ p_3(m - p_1) + p_0, & m \geq p_1, \end{cases} \quad (3)$$

where p_i are parameters. For our hadronic MR curves,

$$R_{\text{hadronic}}(m) \equiv \mathcal{R}(m|p_0, p_1, p_2, p_3), \quad (4)$$

we employ four sets of p_i (models A,B,C,D) listed in Table I, with the associated MR curves plotted in Fig. 2. The large kink in model D emulates a MR curve plateauing as it approaches the maximal mass. For comparison, also shown in the figure are several hadronic MR curves obtained from Refs [25, 33–35].

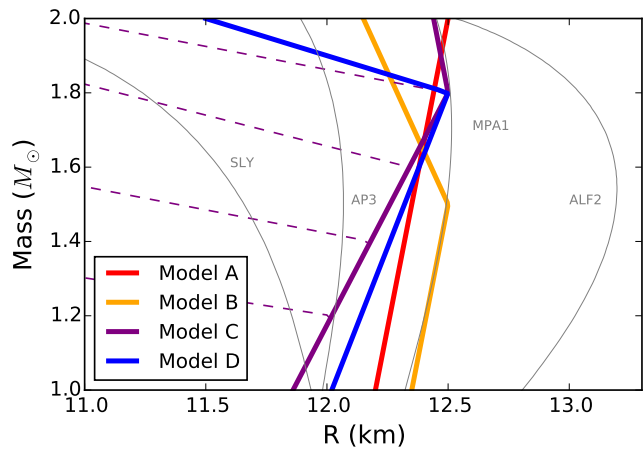


FIG. 2. Four linear piecewise models for $R_{\text{hadronic}}(m)$. For comparison, the MR curves generated with several candidate nuclear EoS are also shown. The purple dashed lines correspond to several hybrid branches of the MR curves.

We focus on HNS with connected MR curves with

$$R_{\text{hybrid}}(m) \equiv \mathcal{R}(m|q_0, m_c, p_2, \alpha), \quad (5)$$

where $q_0 \equiv p_0 - p_2(p_1 - m_c)$. We consider critical mass m_c and hybrid branch slope α [36]

$$m_c = \{1.2, 1.4, 1.6, 1.8\}M_\odot, \quad (6a)$$

$$-\alpha = \{0.5, 1, 2, 4, 6, 8, 10\}\text{km}/M_\odot. \quad (6b)$$

Additionally, we use the same parameters p_0, p_1, p_2 listed Table I and restrict our attention to $m_c \leq p_1$. Note that with this parametrization we have $R_{\text{hybrid}}(m) = R_{\text{hadronic}}(m)$ for $m < m_c$. As such, we refer to hybrid MR curves as “hybrid models A-D with hybrid branch slope α and critical mass m_c ”. Also shown in Fig. 2 are several hybrid branches for model C.

The signal-to-noise ratio (SNR) of the simulated detections follows a power-law distribution valid for nearby events with redshift less than ~ 0.1 (see Refs. [37, 38] for details). For each merger we use the SNR to add Gaussian noise to the *inferred* radius, Eq. (8) below, and masses m_1 such that a GW170817-like event has 1- σ radius and mass uncertainties of 0.75 km and $0.1M_\odot$, respectively [3, 4]. The chirp mass is assumed to be measured with negligible uncertainty.

Data analysis and results.—To analyze our simulated data, it is useful to construct a measure of the NS radius from \mathcal{M} and $\tilde{\Lambda}$. As stated above, $\tilde{\Lambda}$ depends on m_1 , m_2 and the NS radii R_1 and R_2 . To move forward, we make the approximation $R_1 = R_2 \equiv R_{\text{inferred}}$. This approximation is reasonable for purely hadronic NSs, since their MR curves are roughly constant in the $[1, 2]M_\odot$ mass range, but need not be valid for HNS, since their radii need not be constant as Fig. 1 highlights. We will return

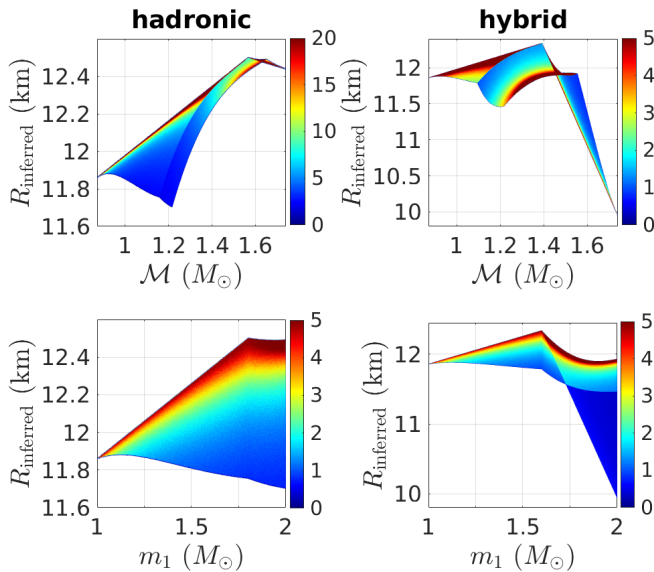


FIG. 3. The density of events in the $\mathcal{M}-R_{\text{inferred}}$ (top) and m_1-R_{inferred} (bottom) planes for hadronic model C (left) and a hybrid model (right) with QM branch slope $\alpha = -6$ and critical mass $m_c = 1.6M_{\odot}$. Outside the shaded regions the densities vanish. Note the presence of kinks in the hybrid allowed regions, which occur at $\mathcal{M} = m_c/2^{1/5}$ and $m_1 = m_c$.

to this issue shortly. With $R_1 = R_2$, the resulting expression for $\tilde{\Lambda}$ is insensitive to the mass ratio $q \equiv m_1/m_2$ [39]. Indeed, at fixed R_{inferred} and for $q \in (1/2, 1)$, $\tilde{\Lambda}$ is nearly constant. It therefore makes sense to expand $\tilde{\Lambda}$ about $q = 1$, which yields

$$\tilde{\Lambda} = \Lambda(2^{1/5}\mathcal{M}/R_{\text{inferred}}) + \mathcal{O}((q-1)^2). \quad (7)$$

Solving for R_{inferred} then yields

$$R_{\text{inferred}} = 2^{1/5}\mathcal{M}/C(\tilde{\Lambda}), \quad (8)$$

where $C(\Lambda)$ is given by Eq. (2).

Since in deriving Eq. 8 we assumed $R_1 = R_2$, R_{inferred} need not be a good estimator of HNS radii, which can vary significantly as a function of mass. Nevertheless, the value of R_{inferred} lies in the fact that as an observable, it is sensitive to kinks in MR curves. To illustrate this, in Fig. 3 we show the density of events in the $\mathcal{M}-R_{\text{inferred}}$ (top) and m_1-R_{inferred} (bottom) planes for hadronic model C (left) and hybrid model C with critical mass $m_c = 1.6M_{\odot}$ and hybrid branch slope $\alpha = -6$ km/ M_{\odot} . The density of events vanishes outside the shaded regions [40]. As is evident from the figure, HNSs produce pronounced kinks in allowed regions, with negative slopes at larger \mathcal{M} and m_1 . In contrast, the allowed regions generated by hadronic model C show no prominent kinks or pronounced downwards trends as \mathcal{M} or m_1 increase.

A simple scheme to search for kinks in the $\mathcal{M}-R_{\text{inferred}}$ and m_1-R_{inferred} planes is simply to fit the data

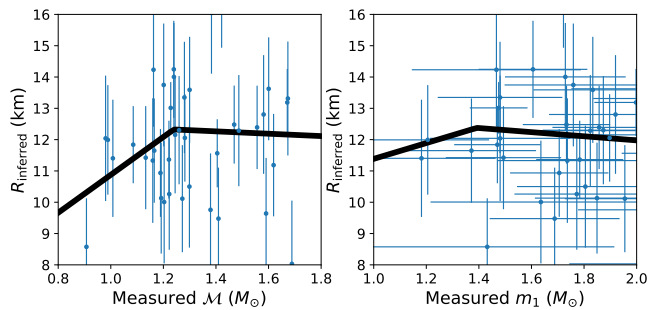


FIG. 4. Left: an example of 40 simulated events in the $\mathcal{M}-R_{\text{inferred}}$ plane for the same hybrid model shown in Fig. 3. Right: the same thing but in the m_1-R_{inferred} plane. The solid lines in both plots are piecewise linear fits.

to linear piecewise models $\mathcal{R}(\mathcal{M}|P_0, P_1, P_2, P_3)$ and $\mathcal{R}(m_1|P_0, P_1, P_2, P_3)$ respectively, with fit parameters P_i and P_i , and \mathcal{R} given by Eq. (3) [41]. In Fig. 4 we show one realization of 40 detections in the measured $\mathcal{M}-R_{\text{inferred}}$ plane (left) and the measured m_1-R_{inferred} plane (right) for the hybrid model shown in Fig. 3. Also shown are the associated piecewise fits. We find that after repeating our simulations 500 times with 40 detections in each simulation, the majority of the simulations with HNSs return negative slope \mathcal{P}_3 . This is in qualitative agreement with the shape of the allowed region in the $\mathcal{M}-R_{\text{inferred}}$ plane shown in Fig. 3 for hybrid data.

In Figure 5, we show the fraction of 500 simulated ensembles which return $\mathcal{P}_3 < 0$ with hybrid injection data with slope α and critical mass m_c . In each ensemble there are 40 simulated events. This quantity measures the confidence a hybrid model with parameters m_c and α can be excluded if $\mathcal{P}_3 > 0$ with 40 BNS detections. As is evident from the figure, smaller critical masses m_c and more negative slopes α can be excluded with greater confidence than larger m_c and/or more positive α . This is due to the fact that more negative α produce larger kinks in the allowed regions in the $\mathcal{M}-R_{\text{inferred}}$ plane, making \mathcal{P}_3 more negative. Likewise, larger m_c leaves fewer events in the $[1, 2]M_{\odot}$ range with masses $> m_c$, making the associated downward trend more difficult to resolve. Nevertheless, it is noteworthy that already with 40 detections, hybrid models with $m_c \leq 1.6M_{\odot}$ and $\alpha \leq -6$ km/ M_{\odot} can be excluded at $> 80\%$ confidence level if $\mathcal{P}_3 > 0$.

On the other hand, with injection data from hadronic models A-D, we find that the majority of our simulations return measured \mathcal{M} slope $\mathcal{P}_3 > 0$ or measured m_1 slope discontinuity $P_2 - P_3 < 1$ km/ M_{\odot} . This selection criterion matches Fig. 3, where the hadronic model produced upwards trends in the $\mathcal{M}-R_{\text{inferred}}$ plane as \mathcal{M} increases and no kinks in the m_1-R_{inferred} plane. In Fig. 6 we plot unity minus the fraction of simulated hadronic ensembles which return $\mathcal{P}_3 < 0$ and $P_2 - P_3 > 1$ km/ M_{\odot}

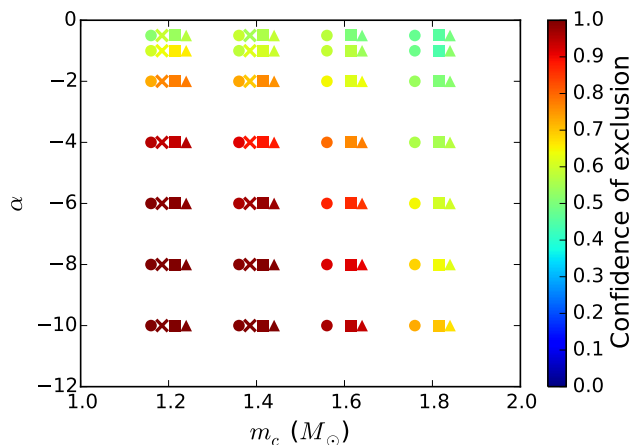


FIG. 5. Confidence of exclusion for hybrid models as function of critical mass m_c and slope α . The four symbols represent our four choices of parameters p_0 and p_2 , which are the same as those listed in Table. I, with circle: model A, cross: model B, square: model C, and triangle: model D.

as a function of the number of events in each ensemble. This quantity can be interpreted as the confidence level of identifying a HNS. Fig. 6 shows the confidence of identifying HNS as a function of the number of detections. Note the confidence of identification does not increase much as the number of events increases (and in fact even decreases slightly). This is due to our strict selection criteria, chosen to prevent misidentification of HNS, as well as the fact that our piecewise linear model only qualitatively describes the distributions shown in Fig. 3. Nevertheless, for the most pessimistic nuclear model, model D, we can construct over 70% confidence of identification with 40 observations if the observations return $\mathcal{P}_3 < 0$ and $P_2 - P_3 > 1$ km/ M_\odot . Since we do not know the actual nuclear MR curve, the results from model D can be conservatively taken as the confidence of identification when our method is applied to real data.

We conclude our analysis by discussing the reconstruction of the critical mass m_c from our simulated data. From Fig. 3 we see that kinks in the allowed regions in the $\mathcal{M}-R_{\text{inferred}}$ and m_1-R_{inferred} plane occur at $\mathcal{M} = m_c/2^{1/5}$ and $m_1 = m_c$, respectively. Therefore, for simulations that are identified as having HNSs, $2^{1/5}\mathcal{P}_1$ and P_1 provide a rough estimate of m_c . In Fig. 7, we show $2^{1/5}\mathcal{P}_1/m_c$ and P_1/m_c as a function of the injected critical mass m_c , averaged over 500 simulations, each with 200 mergers. The standard deviation of \mathcal{P}_1 is $0.05 - 0.4M_\odot$ while the standard deviation of P_1 is $0.3 - 0.5M_\odot$. In addition to the large statistical uncertainty, the figure also shows an estimate of the systematic errors. While the statistical uncertainty decreases over the number of detections, the systematic errors remain. Again, this is because our piecewise linear model only qualitatively describes the distributions shown in Fig. 3.

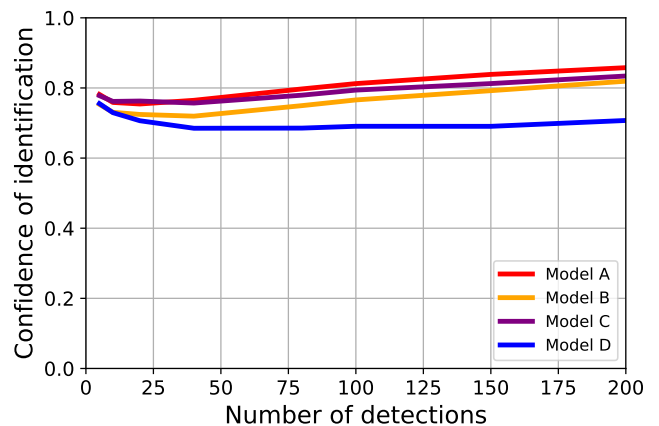


FIG. 6. The confidence of identification of HNSs as a function of the number of detections with our four different hadronic models.

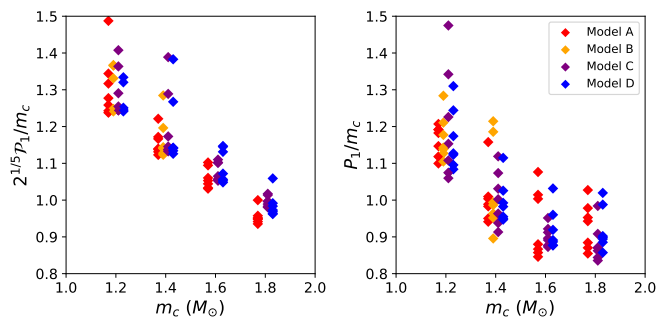


FIG. 7. Estimate of critical mass normalized to the injected value, $2^{1/5}\mathcal{P}_1/m_c$ (left) and P_1/m_c (right), as a function of injected critical mass m_c , from 200 detections identified as having HNSs with our selection criterion.

Discussion.—While we have focused only on HNS with connected MR curves, we have also studied those disconnected MR curves. In this case the allowed regions in the $\mathcal{M}-R_{\text{inferred}}$ and m_1-R_{inferred} planes have gaps, which reflect the presence of gaps in the associated MR curves. Our present analysis cannot resolve these gaps, but can resolve the change in slope associated with the formation of a core with similar fidelity as reported above for connected models. In the future, it would also be interesting to study the models with a mixed phase of hadronic and QM. This scenario arises when the hadronic matter/QM surface tension is small. The presence of a mixed phase should soften kinks in MR curves, and correspondingly those in the m_1-R_{inferred} and $\mathcal{M}-R_{\text{inferred}}$ planes. It remains to be seen how soft of a kink our analysis can detect.

We note that the selection criterion used to identify HNSs is not unique. While using a stronger selection criterion might, for a given number of events, identify HNSs with greater confidence, it might also misidentify more HNSs as hadronic than a weaker criterion.

There is plenty room to improve our data analysis. Firstly, we assumed a uniform NS mass distribution between $[1, 2]M_{\odot}$. Employing a different mass distribution will affect the fidelity in which HNS can be probed. For example, if $m_c = 1.6M_{\odot}$ and the NS mass distribution is narrowly distributed about $1.4M_{\odot}$, identifying QM cores will be very difficult due to few high mass events. As more and more gravitational wave events are detected, the mass distribution should be better understood, and our analysis can be adjusted accordingly.

Additionally, our analysis of data in the $\mathcal{M}-R_{\text{inferred}}$ and m_1-R_{inferred} planes can likely be improved. For example, instead of fitted data to piecewise linear curves $\mathcal{R}(\mathcal{M}|\mathcal{P}_0, \mathcal{P}_1, \mathcal{P}_2, \mathcal{P}_3)$ and $\mathcal{R}(m_1|P_0, P_1, P_2, P_3)$, it may be fruitful to fit instead to the *density* of expected events, which is determined by the mass distribution and the MR curve. This requires knowledge of the NS mass distribution. Fitting to the density of events can likely ameliorate the aforementioned systematic errors on the measurement of the critical mass.

Acknowledgments.—We acknowledge valuable discussions with Katerina Chatziioannou, Ian Harry, Carl-Johan Haster, Philippe Landry, Jocelyn Read, and Salvatore Vitale. This work was supported by the Black Hole Initiative at Harvard University, which is funded by grants the John Templeton Foundation and the Gordon and Betty Moore Foundation to Harvard University.

* hsin-yu.chen@fas.harvard.edu

† pchesler@g.harvard.edu

‡ aloeb@cfa.harvard.edu

- [1] B. P. Abbott, R. Abbott, T. D. Abbott, F. Acernese, K. Ackley, C. Adams, T. Adams, P. Addesso, R. X. Adhikari, V. B. Adya, and et al., “GW170817: Observation of Gravitational Waves from a Binary Neutron Star Inspiral,” *Phys. Rev. Lett.* **119** (Oct, 2017) 161101, [arXiv:1710.05832 \[gr-qc\]](#).
- [2] B. P. Abbott, R. Abbott, T. D. Abbott, F. Acernese, K. Ackley, C. Adams, T. Adams, P. Addesso, R. X. Adhikari, V. B. Adya, and et al., “Multi-messenger Observations of a Binary Neutron Star Merger,” *Astrophys. J. Lett.* **848** (Oct, 2017) L12, [arXiv:1710.05833 \[astro-ph.HE\]](#).
- [3] B. P. Abbott, R. Abbott, T. D. Abbott, F. Acernese, K. Ackley, C. Adams, T. Adams, P. Addesso, R. X. Adhikari, and V. B. Adya, “GW170817: Measurements of Neutron Star Radii and Equation of State,” *Phys. Rev. Lett.* **121** (Oct, 2018) 161101, [arXiv:1805.11581 \[gr-qc\]](#).
- [4] B. P. Abbott, R. Abbott, T. D. Abbott, F. Acernese, K. Ackley, C. Adams, T. Adams, P. Addesso, R. X. Adhikari, and V. B. Adya, “Properties of the Binary Neutron Star Merger GW170817,” *Physical Review X* **9** (Jan, 2019) 011001, [arXiv:1805.11579 \[gr-qc\]](#).
- [5] B. P. Abbott, R. Abbott, T. D. Abbott, M. R. Abernathy, F. Acernese, K. Ackley, C. Adams, T. Adams, P. Addesso, R. X. Adhikari, and et al., “Prospects for observing and localizing gravitational-wave transients with Advanced LIGO, Advanced Virgo and KAGRA,” *Living Reviews in Relativity* **21** (Apr, 2018) 3, [arXiv:1304.0670 \[gr-qc\]](#).
- [6] E. Annala, T. Gorda, A. Kurkela, and A. Vuorinen, “Gravitational-wave constraints on the neutron-star-matter Equation of State,” *Phys. Rev. Lett.* **120** (2018) no. 17, 172703, [arXiv:1711.02644 \[astro-ph.HE\]](#).
- [7] E. R. Most, L. R. Weih, L. Rezzolla, and J. Schaffner-Bielich, “New constraints on radii and tidal deformabilities of neutron stars from GW170817,” *Phys. Rev. Lett.* **120** (2018) no. 26, 261103, [arXiv:1803.00549 \[gr-qc\]](#).
- [8] I. Tews, J. Margueron, and S. Reddy, “Confronting gravitational-wave observations with modern nuclear physics constraints,” *Eur. Phys. J. A* **55** (2019) no. 6, 97, [arXiv:1901.09874 \[nucl-th\]](#).
- [9] M. M. Forbes, S. Bose, S. Reddy, D. Zhou, A. Mukherjee, and S. De, “Constraining the neutron-matter equation of state with gravitational waves,” [arXiv:1904.04233 \[astro-ph.HE\]](#).
- [10] Z. Carson, A. W. Steiner, and K. Yagi, “Future Prospects for Constraining Nuclear Matter Parameters with Gravitational Waves,” [arXiv:1906.05978 \[gr-qc\]](#).
- [11] T. Gorda, A. Kurkela, P. Romatschke, M. Säppi, and A. Vuorinen, “Next-to-Next-to-Next-to-Leading Order Pressure of Cold Quark Matter: Leading Logarithm,” *Phys. Rev. Lett.* **121** (2018) no. 20, 202701, [arXiv:1807.04120 \[hep-ph\]](#).
- [12] Z. F. Seidov, “The Stability of a Star with a Phase Change in General Relativity Theory,” *Soviet Astronomy* **15** (Oct., 1971) 347.
- [13] R. Schaeffer, L. Zdunik, and P. Haensel, “Phase transitions in stellar cores. i - equilibrium configurations,” *Astronomy and Astrophysics* **126** (1983) no. 1, 121–145. <http://search.proquest.com/docview/23299272/>.
- [14] L. Lindblom, “Phase transitions and the mass radius curves of relativistic stars,” *Phys. Rev.* **D58** (1998) 024008, [arXiv:gr-qc/9802072 \[gr-qc\]](#).
- [15] K. Yagi and N. Yunes, “Approximate Universal Relations for Neutron Stars and Quark Stars,” *Phys. Rept.* **681** (2017) 1–72, [arXiv:1608.02582 \[gr-qc\]](#).
- [16] M. G. Alford, K. Rajagopal, S. Reddy, and F. Wilczek, “The Minimal CFL nuclear interface,” *Phys. Rev.* **D64** (2001) 074017, [arXiv:hep-ph/0105009 \[hep-ph\]](#).
- [17] M. G. Alford and S. Han, “Characteristics of hybrid compact stars with a sharp hadron-quark interface,” *Eur. Phys. J. A* **52** (2016) no. 3, 62, [arXiv:1508.01261 \[nucl-th\]](#).
- [18] M. G. Alford, S. Han, and M. Prakash, “Generic conditions for stable hybrid stars,” *Phys. Rev.* **D88** (2013) no. 8, 083013, [arXiv:1302.4732 \[astro-ph.SR\]](#).
- [19] E. Annala, T. Gorda, A. Kurkela, J. Nättilä, and A. Vuorinen, “Quark-matter cores in neutron stars,” [arXiv:1903.09121 \[astro-ph.HE\]](#).
- [20] M. G. Alford, S. Han, and K. Schwenzer, “Signatures for quark matter from multi-messenger observations,” [arXiv:1904.05471 \[nucl-th\]](#).
- [21] A. Bauswein, N.-U. F. Bastian, D. B. Blaschke, K. Chatziioannou, J. A. Clark, T. Fischer, and

- M. Oertel, “Identifying a first-order phase transition in neutron star mergers through gravitational waves,” *Phys. Rev. Lett.* **122** (2019) no. 6, 061102, [arXiv:1809.01116 \[astro-ph.HE\]](#).
- [22] E. R. Most, L. J. Papenfort, V. Dexheimer, M. Hanauske, S. Schramm, H. Stöcker, and L. Rezzolla, “Signatures of quark-hadron phase transitions in general-relativistic neutron-star mergers,” [arXiv:1807.03684 \[astro-ph.HE\]](#).
- [23] A. W. Steiner, C. O. Heinke, S. Bogdanov, C. Li, W. C. G. Ho, A. Bahramian, and S. Han, “Constraining the Mass and Radius of Neutron Stars in Globular Clusters,” *Mon. Not. Roy. Astron. Soc.* **476** (2018) no. 1, 421–435, [arXiv:1709.05013 \[astro-ph.HE\]](#).
- [24] S. Benic, D. Blaschke, D. E. Alvarez-Castillo, T. Fischer, and S. Typel, “A new quark-hadron hybrid equation of state for astrophysics - I. High-mass twin compact stars,” *Astron. Astrophys.* **577** (2015) A40, [arXiv:1411.2856 \[astro-ph.HE\]](#).
- [25] H. Mütter, M. Prakash, and T. L. Ainsworth, “The nuclear symmetry energy in relativistic Brueckner-Hartree-Fock calculations,” *Phys. Lett.* **B199** (1987) 469–474.
- [26] J. Antoniadis *et al.*, “A Massive Pulsar in a Compact Relativistic Binary,” *Science* **340** (2013) 6131, [arXiv:1304.6875 \[astro-ph.HE\]](#).
- [27] H. T. Cromartie *et al.*, “A very massive neutron star: relativistic Shapiro delay measurements of PSR J0740+6620,” [arXiv:1904.06759 \[astro-ph.HE\]](#).
- [28] B. Carr and F. Kuhnel, “Primordial black holes with multimodal mass spectra,” *Phys. Rev.* **D99** (2019) no. 10, 103535, [arXiv:1811.06532 \[astro-ph.CO\]](#).
- [29] H.-Y. Chen and K. Chatziioannou, “Distinguishing binary neutron star from neutron star-black hole mergers with gravitational waves,” *arXiv e-prints* (Mar, 2019) [arXiv:1903.11197](#), [arXiv:1903.11197 \[astro-ph.HE\]](#).
- [30] F. Özel and P. Freire, “Masses, Radii, and the Equation of State of Neutron Stars,” *Ann. Rev. Astron. Astrophys.* **54** (2016) 401–440, [arXiv:1603.02698 \[astro-ph.HE\]](#).
- [31] A. Maselli, V. Cardoso, V. Ferrari, L. Gualtieri, and P. Pani, “Equation-of-state-independent relations in neutron stars,” *Phys. Rev.* **D88** (2013) no. 2, 023007, [arXiv:1304.2052 \[gr-qc\]](#).
- [32] Z. Carson, K. Chatziioannou, C.-J. Haster, K. Yagi, and N. Yunes, “Equation-of-state insensitive relations after GW170817,” *Phys. Rev.* **D99** (2019) no. 8, 083016, [arXiv:1903.03909 \[gr-qc\]](#).
- [33] F. Douchin and P. Haensel, “A unified equation of state of dense matter and neutron star structure,” *Astron. Astrophys.* **380** (2001) 151, [arXiv:astro-ph/0111092 \[astro-ph\]](#).
- [34] A. Akmal, V. R. Pandharipande, and D. G. Ravenhall, “The Equation of state of nucleon matter and neutron star structure,” *Phys. Rev.* **C58** (1998) 1804–1828, [arXiv:nucl-th/9804027 \[nucl-th\]](#).
- [35] M. Alford, M. Braby, M. W. Paris, and S. Reddy, “Hybrid stars that masquerade as neutron stars,” *Astrophys. J.* **629** (2005) 969–978, [arXiv:nucl-th/0411016 \[nucl-th\]](#).
- [36] We note that recently Ref. [19] has claimed there can be no HNSs below $1.44M_{\odot}$. However, it is easy to come up with counterexample QM EoSs consistent with the assumptions of Ref. [19] that yield HNS even below $1M_{\odot}$.
- [37] B. F. Schutz, “Networks of gravitational wave detectors and three figures of merit,” *Classical and Quantum Gravity* **28** (Jun, 2011) 125023, [arXiv:1102.5421 \[astro-ph.IM\]](#).
- [38] H.-Y. Chen and D. E. Holz, “The Loudest Gravitational Wave Events,” *arXiv e-prints* (Sep, 2014) [arXiv:1409.0522](#), [arXiv:1409.0522 \[gr-qc\]](#).
- [39] C. Raithel, F. Özel, and D. Psaltis, “Tidal deformability from GW170817 as a direct probe of the neutron star radius,” *Astrophys. J.* **857** (2018) no. 2, L23, [arXiv:1803.07687 \[astro-ph.HE\]](#).
- [40] Note the densities in some regions go off the color scale.
- [41] The fitting was done with a 2-step χ^2 minimization. First, we search for a minimum of χ^2 on a coarse grid of parameters \mathcal{P}_i or P_i ([Lower bound, Upper bound, Number of grids in between] for the four parameters, respectively): [10km, 13km, 6], [1.0 M_{\odot} , 2.0 M_{\odot} , 10], [−3km/ M_{\odot} , 3km/ M_{\odot} , 12], [−45km/ M_{\odot} , 12km/ M_{\odot} , 50]. We then use `scipy.optimize.leastsq` function in `python` to find the best fit parameters.